A model-based correction method for beam hardening artefacts in X-ray microtomography

E Van de Casteele, D Van Dyck, J Sijbers ‡ and E Raman

Vision Lab, Physics Department, University of Antwerp (RUCA), Belgium

Abstract. In micro computer tomography (μCT) and medical CT, X-ray sources are polychromatic. Because of this polychromaticity, Beer's law, which states that the ratio of the attenuated and incoming X-ray beam is exponential with the thickness of the material, is no longer valid. This leads to quantitative and visual errors in the reconstructed images, e.g. cupping and streak artefacts.This paper describes a correction scheme for these artefacts using a bimodal energy model for the source-detector energy spectrum. In essence, this correction procedure is a linearization technique based on a physical model instead of the use of polynomials. The results are obtained for different test objects made of combinations of plexiglas, bone, water and aluminium. They demonstrated the effectiveness of the bimodal model correcting for the beam hardening artefact in two-, and multi-component systems.

Keywords: Microtomography, beam hardening correction, bimodal energy model

E-mail: `elke.vandecasteele@ua.ac.be`

1. Introduction

X-ray computer tomography (CT) and microtomography enables nondestructive visualization of the internal structure of objects. In addition, CT allows quantitative analysis of the thickness or composition of the material. However, the accuracy of the reconstructed CT values assumes that the attenuation of the incident X-ray beam is exponentially related to the thickness of the object, cfr. Beer's law. This relationship will no longer hold as a consequence of the polychromaticity of the source used in both medical CT and μCT. Because of the energy dependence of the attenuation coefficient, the different energy levels of the polychromatic spectrum are not attenuated in the same way. Indeed, the lower energies will be easily absorbed, while the higher or harder energies are less attenuated. In other words, lower energy photons are removed preferentially from the X-ray beam spectrum as it passes through the object, resulting in a process called beam hardening. Therefore, the intensities in the projection images are not proportional to the object thickness, causing pronounced edges, streaks, and environmental artefacts in the reconstructed image [2, 3, 11, 14].

The importance of the problem of correcting for beam hardening in computer tomography is reflected in the large number of publications that have appeared on this topic. These correction methods can be divided in three main classes: hardware filtering, linearization, and dual energy.

- Hardware filtering is by far the most popular method to reduce the beam hardening effect [8]. By placing a filter between the source and the object, such as a thin aluminium plate, the low energy X-rays are absorbed before the beam reaches the material. The main disadvantage of this technique is the decreased amount of X-rays, which results in a decrease of the image signal-to-noise ratio (SNR). Furthermore, this method gives only a reduction of the beam hardening effect.

- A second, commonly applied correction method is based on a linearization procedure [2, 5, 6]. Here, the measured nonlinear relationship between object thickness and the log ratio of the intensities is fitted with polynomials. Correcting every point lying along the polynomial towards the linear trendline will eliminate the beam hardening artefact. For only small beam hardening artefacts, as observed in medical scans of soft tissues, a second order polynomial fit is adequate [6]. However, for more severe artefacts, as in denser materials, polynomial degrees of eight or higher are required [5]. The linearization procedure with polynomials has the advantage that the coefficients are easy to calculate and, once they are calculated, it is easy to correct the beam hardening effect. For systems consisting of more than two components, this method is often used in combination with the projection data and a first reconstruction image to obtain more prior information about the object under investigation [7, 9, 10].

- The last correction method is called dual energy [1, 4]. Dual energy offers the possibility to image the photoelectric effect and the Compton scattering, separately. Images in tomography represent the attenuation coefficient, which is often difficult to interpret because it is a combination of the atomic number Z, the material density ρ, and the X-ray energy E. With dual energy, two scans are acquired: one at low and one at high peak voltage. We may choose to image the photoelectric effect, which depends strongly on the atomic number Z and thus provides an indication of the composition of the object. On the other hand, the Compton scattering coefficient depends on the material density ρ. However, the technique has the disadvantage of being complex, difficult to implement and very sensitive to noise. Furthermore, it requires two consecutive exposures, which increases the recording time and dose.

In this paper, a physical model, recently introduced by Van de Casteele *etal* (2002)[12], is

applied to account for the beam hardening effect of different materials and compositions. In essence, this correction scheme is a linearization procedure. Furthermore, from the fact that a physical model is used, the fitting parameters have also a physical meaning which can be used to obtain more information about the source-detector efficiency.

2. Theory

To understand the correction procedure applied in this paper, a brief explanation of the main concepts of the bimodal energy model, used to describe the beam hardening curve, is appropriate. A beam hardening curve represents the relation between the object thickness d and the logarithm of the ratio of incoming I_0 and attenuated X-ray intensity I (further referred to as the attenuation or attenuation values). The bimodal energy model is based on the approximation that the detected energy spectrum is characterized by two dominant energies, E_1 and E_2. Although a bimodality in the source-detector efficiency is assumed, the exact knowledge of the source spectrum is not required. First of all, the bimodality is an approximation which may be generally assumed as a consequence of the two different parts in the detector efficiency curves before and after the absorption edges (cfr. figure 1). In our case, the choice of source-detector system will enhance this assumption. This may be justified by inspecting the peak energies of the tungsten (W) X-ray source and the gadox (Gd_2O_2S) detector. The detector efficiency $\gamma(E)$ and source spectrum $f(E)$ are depicted in figures 1 and 2. As shown in Van de Casteele *etal* (2002) [12], this particular combination of source and scintillator material gives rise to two bands in the energy spectrum, which led to the proposition of a bimodal form for the detected energy distribution. The attenuation as a function of the object thickness is then given by:

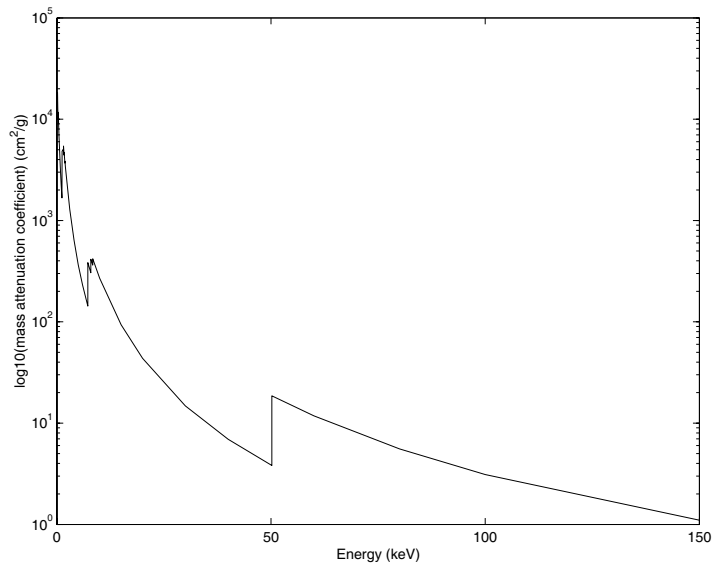$$\ln \frac{I_0}{I} = \mu_2 d + \ln \left[\frac{1 + \alpha}{1 + \alpha e^{-(\mu_1 - \mu_2)d}} \right] \tag{1}$$

Figure 1. The detector efficiency of a gadox (Gd_2O_2S) detector produces two attenuation edges of the K and L shells of the scintillator material. Notice the two regions before and after the 50 keV (electron energy) which delivers the general assumption of the bimodality.
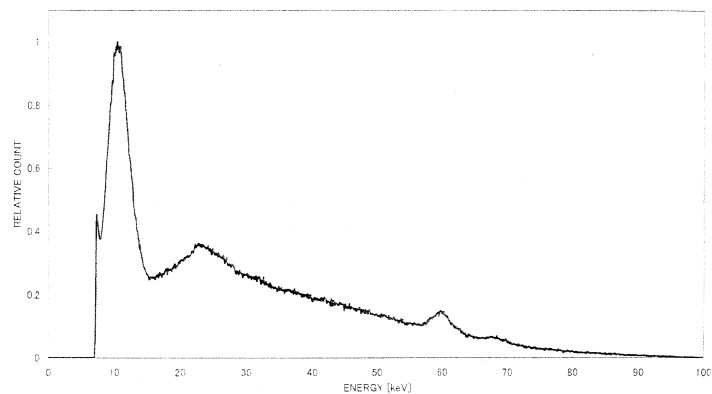

Figure 2. L 8032 Spectral distribution measured by Hamamatsu of a source with tungsten (W) as target material and a tube voltage of 100 kVp. This target material is used in our Skyscan-1072 system with a source voltage of 80 kVp.

where μ is the attenuation coefficient with $\mu_1 = \mu(E_1)$ and $\mu_2 = \mu(E_2)$, and α the ratio of the source-detector efficiency $f(E)\gamma(E)$ at energy E_1 and E_2. It was shown in [12] that this model accurately fits the experimental beam hardening curve for various materials.

3. Materials and methods

3.1. Phantoms and test objects

In this paper, we will call the objects made for the purpose of constructing the beam hardening curve, phantoms, while the objects subjected to CT examination are referred to as test objects. The phantoms are made of material with an attenuation range close to that of the test object. Ideally, the same material as the object should be used to determine the beam hardening curves. Phantoms are constructed as to examine the attenuation of a certain material as a function of its thickness. Phantoms are either plates with a known thickness or wedge-shaped.

The test objects were composed of plexiglas, water, aluminium, and bone. Plexiglas is often used to create test objects representing biological soft tissue or water [3]. The material density of plexiglas equals 1.19 g/cm^3, while the densities of soft tissue and water are 1.06 g/cm^3 and 1.00 g/cm^3, respectively. Plexiglas was studied in a two-component system of plexiglas and air, and in combination with water forming a three-component system, to justify the assumption of plexiglas as a reference material for water and soft tissues in X-ray tomography.

Most bone studies in μCT take place on either bone in air or immersed in a water or oil solution. As a consequence of the rising temperature inside the microtomograph, fresh bones will dry out when they are not immersed in a proper solution. The density of bone is 1.92 g/cm^3, thus the beam hardening artefacts for bone are more severe than for soft tissues. Here, the femur of a mouse was used to test the correction procedure for a two- and multi-component system. However, before studying the system of bone in a water solution, a test object of plexiglas and aluminium was created to demonstrate the effectiveness of the bimodal model in correcting beam hardening artefacts in a multi-component system. Here the surrounding plexiglas, which was the outer material, is

considered as a filter between the source and the aluminium. Aluminium (2.70 g/cm^3) has a higher material density than bone, thus even more severe cupping artefacts are obtained.

3.2. Apparatus

The experiments were performed on the "Skyscan-1072" system. This is a desktop X-ray microfocus computer tomography system, which has been commercialized by Skyscan§, a spin-off company of the University of Antwerp. It contains a 80 kVp Hamamatsu X-ray source (with a tungsten target and a focal spot size of 8μm) and a gadox (Gd_2O_2S) scintillator with a 3.7:1 fibre optics coupling to a 1024 × 1024 12-bit cooled CCD camera. The test object was placed on a sample holder between the detector and the X-ray source. As a consequence of the cone beam, produced by the source, the distance of the sample to the source determines the magnification of the system. The rotation step was set at 0.9 °, which corresponds with 200 views or projections for acquisitions around 180 ° (+ fan angle for reconstruction purposes) . The field of view was limited to 25 mm. The projection data were sorted in a sinogram of size 1024 × 200, where every column represents the attenuation data from one slice along one direction. The sinograms are used to reconstruct the attenuation data applying a fan beam algorithm. The images in this paper were taken at maximum tube voltage, thus 80 kVp, and exposure times of 2 seconds.

3.3. Methods

The correction procedure depends on the composition of the test object under investigation. The simplest case is a test object consisting of only one material. This is called a two-component system (air and the test object material). Before correcting the

§ http://www.skyscan.be

attenuation values in the sinogram of the test object, the beam hardening curve of the material has to be determined. For this purpose, phantoms were used. The phantoms are either wedge-shaped or thin plates, which are consecutively stacked to examine the attenuation values at different thicknesses. These attenuation values are calculated as $\ln(I_0/I)$ by measuring the incident intensity I_0 and the resulting, attenuated intensity I in the shadow images taken of the phantoms. Applying wedge-shaped phantoms has the advantage that only one projection image is required to obtain more data points on the beam hardening curve than with the use of plates, which is illustrated in figure 3. The thin plates, used in our experiments, have a thickness of 0.1 mm. Projection images were taken for every consecutively stacked plate. Thus, a beam hardening curve with maximum thickness 1 mm has only 10 data points. However, using a wedge-shaped phantom, it is possible to calculate thicknesses per image pixel value. The thicknesses D_i of the wedge-shaped phantom per pixel are calculated as follows (see figure 3):

$$D_i = (B - i\Delta)\tan\beta \qquad i = 0, \ldots, N \tag{2}$$

where the adjacent side B and the angle β formed by B and the hypotenuse are indicated on figure 3B, i is zero at the opposite side of β, Δ is the pixelsize, and N represents the number of pixels along the phantom.

However, for some test objects, such as bone, it is not possible to make plate or wedge-shaped phantoms. In this case, the beam hardening curve was constructed using the information in the reconstructed CT image. By thresholding the greyvalues in the reconstruction image, the test object is segmented. The segmentation result is then used to calculate the thickness of the test object along the different projection angles (cfr. figure 6). The corresponding attenuation values for the different thicknesses are found in the sinogram. In this way, the beam hardening curve is obtained.
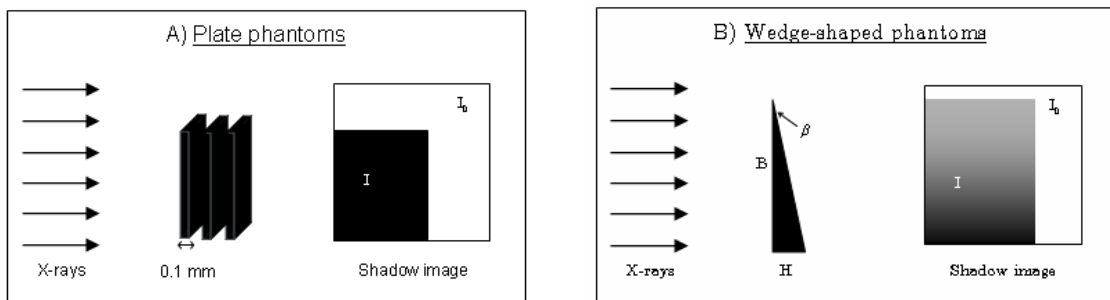
Figure 3. Phantoms are used to determine the data points on the beam hardening curve. A) Three plate phantoms of 0.1 mm each are consecutively stacked and shadow images are taken to calculate the attenuation values $(\ln(I_0/I))$ in function of the thickness. B) Wedge-shaped phantoms need only one projection image which delivers more data points at once in comparison with the plate phantoms.

After determining the relation between object thickness and attenuation of the material, either using phantoms or a first reconstruction image, the model given by equation (1) is fitted with a least-squares method to the experimental data points. The fitting parameters are μ_1, μ_2, and α.

Finally, the projection data in the sinogram is linearized by correcting the attenuation values towards the linear trendline. This gives a new, corrected sinogram which is then reconstructed. The final image is free of beam hardening artefacts.

In a multi-component system, the correction procedure is more complex. In this case a distinction must be made between materials with similar or differing attenuations. An example of two materials with similar attenuation is plexiglas and water. Here the sinogram is corrected using the beam hardening curve of one material. The correction procedure proceeds then in the same way as in the case of a two-component system. When the materials have different attenuations, the correction method becomes iterative. A first reconstruction is made and the different materials in the image are segmented. Then, starting with the outer material, the thicknesses are determined along

one direction using the segmentation image. Only the lines where the X-rays travelled through this material alone are considered. The corresponding attenuation values are found in the sinogram. When more data points on the curve are needed, the thicknesses are calculated along other directions. In this way, the beam hardening curve of the outer material is determined and the corresponding attenuation values are corrected. Note that, if phantoms are available for the outer material, these can be used to determine the beam hardening curve instead of the data from a first reconstruction image. Subsequently, the beam hardening curve of the next material is determined using the segmented image. The outer material will then work as a filter in front of the second material under investigation. In other words, the attenuation values found for a certain thickness of the second material will be higher than without filtering. To obtain the exact beam hardening function for this material, the values on the curve have to be corrected with the attenuation values of the outer material, corresponding to the path where the X-rays had to go through before reaching the second material. The corresponding attenuation values in the sinogram are then linearized. If there are more than two materials, this procedure will go on in the same way for the next material. When all the attenuation values in the sinogram are corrected a new reconstruction image is made. This correction procedure is schematically presented in figure 4.
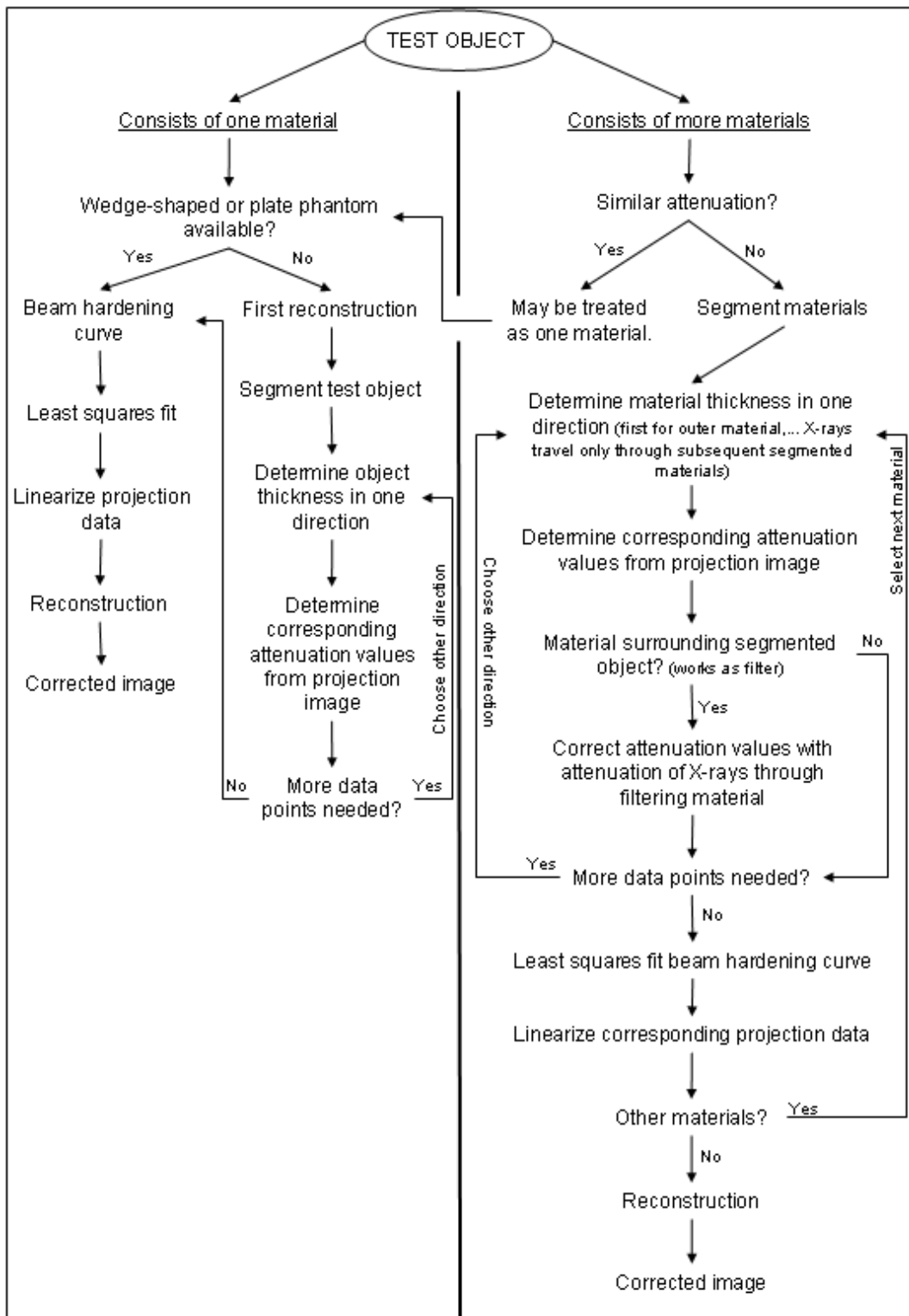
Figure 4. Correcting beam hardening artefacts in two- and multi-component systems.

4. Results

4.1. Beam hardening correction for one material

First of all, the correction method was tested on a two-component system consisting of plexiglas and air. To form the beam hardening curve for plexiglas, a projection image was taken of a wedge-shaped phantom without pre-filtering.

The test object under examination was a plexiglas cylinder with a diameter of 10 mm. This test object was scanned with a magnification of $19.83\times$, which gives a pixel resolution of 13.79 μm in the reconstruction images. Using the fitted beam hardening curve (presented in Van de Casteele *etal* 2002 [12]), the attenuation values of this cylinder found in the sinogram were corrected. In figure 5, the reconstruction images are presented before and after beam hardening correction. To make a comparison with the correction results obtained by hardware filtering, a second experiment was done with a filter of 1 mm aluminium. Such a filter can be applied in μCT to reduce the beam hardening in light materials, such as plexiglas. The correction results are shown in figure 5 and compared with the attenuation profiles through the reconstruction images before and after bimodal energy correction without pre-filtering.

Secondly, we examined how well the beam hardening artefacts are corrected in biological objects. As test object, the femur of a mouse was chosen, which was scanned with a magnification of $33.46\times$, producing a pixel resolution of 8.17 μm. The scans were made at the top of the bone where, in this case, the bone was hollow. In this situation, as explained before (cfr. Methods), the nonlinear curve could not be obtained using a wedge-shaped phantom nor by the use of plates made of the same test object material, thus bone. Therefore, the beam hardening curve was constructed using the information from a first reconstruction image shown in figure 6A. By thresholding the greyvalues, the bone in the reconstruction image was segmented (figure 6B). The thicknesses were
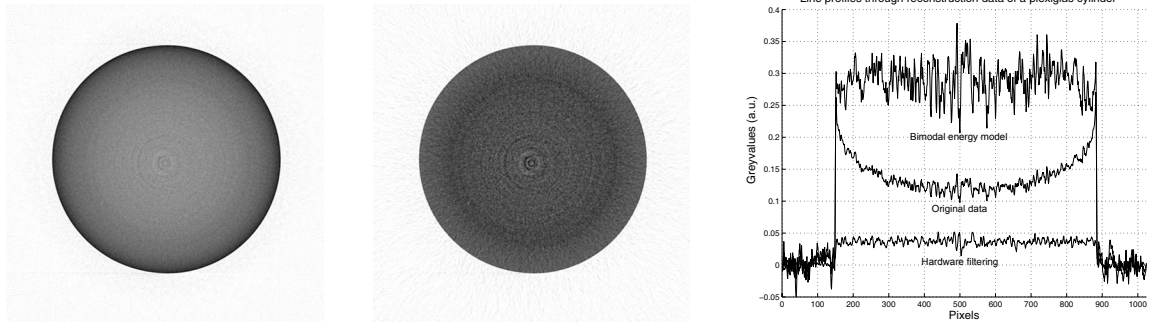
Figure 5. Reconstruction images of a homogeneous plexiglas cylinder of 10 mm in diameter before (left) and after (middle) beam hardening correction. Note that the greyvalues in the reconstructed images are scaled between zero and their maximum. The attenuation profiles (right) through these reconstructions are shown and the bimodal energy correction is compared with the results obtained with a 1 mm aluminium hardware filter.
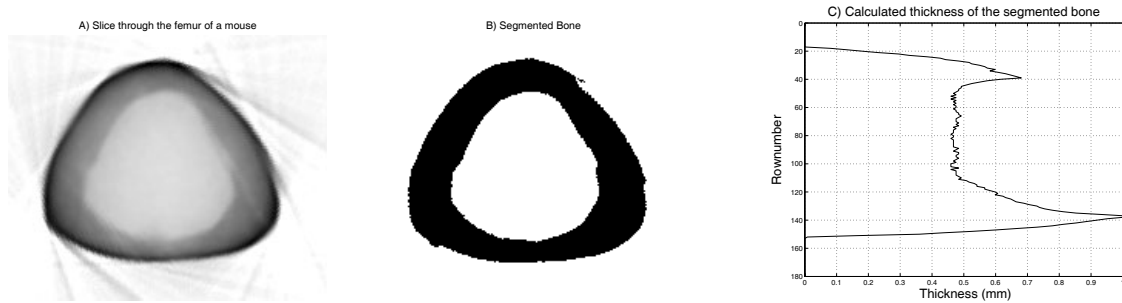

Figure 6. A) Original reconstruction data of a slice through the femur of a mouse. B) Binary image obtained after thresholding the reconstructed image. C) By integrating along the row direction, the thicknesses of the bone are calculated.

calculated by integrating along a given direction and multiplying with the pixel size. The obtained projection curve is depicted in figure 6C. The corresponding attenuation values were found in the sinogram. To obtain more data points, two projections were used along the angles of 0° and 90°, respectively. In this case, the thicknesses could be determined along the row and column direction, respectively. In figure 7, the resulting beam hardening curve for bone is shown. After the determination of the fitting parameters, the beam hardening curve is used to correct the attenuation values in the sinogram. In figure 8, the reconstructed images of a slice through the femur of a
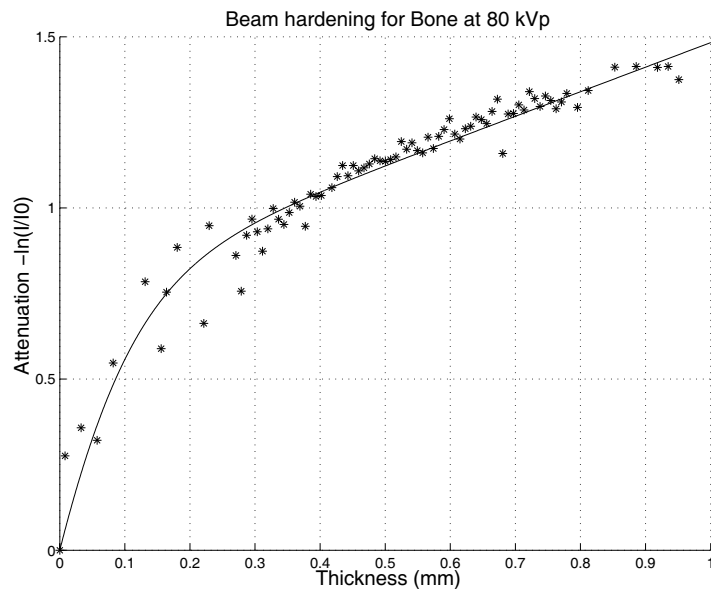
Figure 7. The beam hardening curve for bone at 80 kVp. In this case the thicknesses cannot be obtained using plates or wedge-shaped phantoms of bone. They are calculated from a first reconstruction image made of the uncorrected data.

Figure 8. The attenuation profiles (right) and reconstructed images of a bone, before (left) and after (middle) beam hardening correction. Note that the greyvalues in the reconstructed images are scaled between zero and their maximum value.

mouse are shown as well as the attenuation profiles through the reconstruction images, before and after correction.

4.2. Beam hardening correction for a multi-component system

4.2.1. Materials with similar attenuation When the two materials under examination attenuate the X-rays in almost the same energy range, the beam hardening curve of one of the two materials is used for correcting the artefacts of both materials. Consider for example a combination of plexiglas and water. For this purpose, a test object was created consisting of a plexiglas cylinder with 10 mm in diameter with a hole of 4 mm filled with water in the center. This test object was scanned at a magnification of 19.83×, which results in a pixel resolution of 13.79 μm. Figure 9 shows a line profile through the uncorrected and corrected reconstruction image.
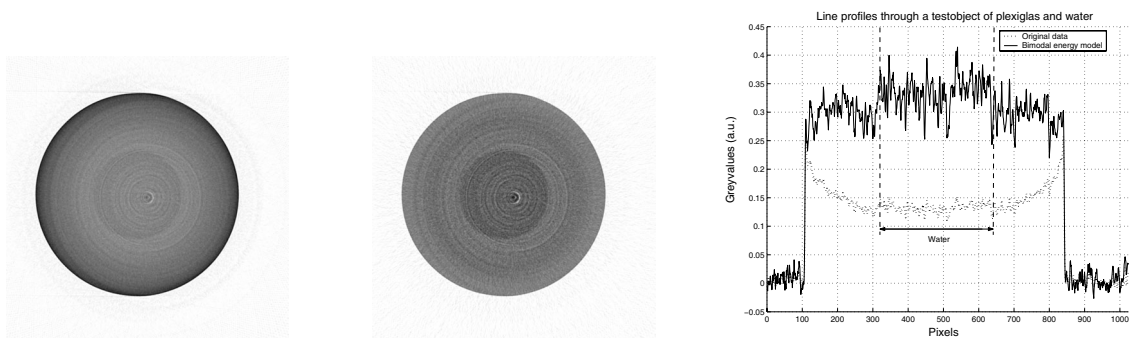

Figure 9. Attenuation profiles (right) and reconstructed images of a test object containing plexiglas and water are shown before (left) and after (middle) beam hardening correction. Note that the greyvalues in the reconstructed images are scaled between zero and their maximum value.

4.2.2. Materials with different attenuations When the attenuation ranges differ significantly, as for plexiglas and aluminium, the beam hardening curves of both materials have to be used. We will perform the beam hardening correction procedure for a test object composed of a plexiglas cylinder of 10 mm diameter and an aluminium rod of 2 mm in the middle of the plexiglas. The test object was scanned with a magnification of 19.83× (pixel resolution 13.79 μm).

The beam hardening curves were obtained as described in section 3.3. The outer
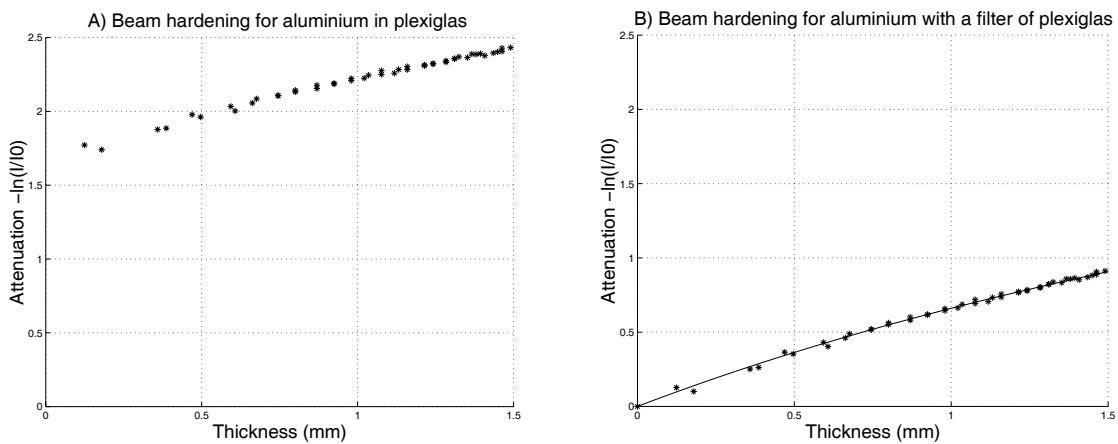
Figure 10. A) The beam hardening curve of aluminium in plexiglas at a peak voltage of 80 kVp. B) We may interpret these data as the attenuation values of aluminium using a plexiglas filter. Here the attenuation of the plexiglas filter is subtracted from the attenuation values of aluminium.

material of this test object was plexiglas. The beam hardening curve of plexiglas was already obtained previously (cfr. section 4.1). When the attenuation values of aluminium, being the second material, are shown as function of the thicknesses, calculated from the segmentation image, the beam hardening curve of figure 10A is obtained. Clearly, for aluminium of zero thickness, the attenuation value will not decrease to zero because of the surrounding plexiglas. In figure 10B, we interpreted the attenuation values as the beam hardening for aluminium using a plexiglas filter, which means that the attenuation value of the surrounding plexiglas is set to zero. This plexiglas filter corresponds with the thickness of the plexiglas where the X-ray beam had to pass before the aluminium is reached. Every point was reduced with the attenuation value of plexiglas for the corresponding thickness. After this subtraction, the beam hardening curve of figure 10B is obtained, which was used to correct the attenuation values of aluminium.

Now the beam hardening curves are known for both plexiglas and aluminium, the correction can be performed. Herefore, every value in the sinogram corresponding to

aluminium was corrected for the exact thickness of plexiglas surrounding the aluminium rod. Figure 11 shows the line profiles and the reconstructed images before and after beam hardening correction. To make a comparison with the correction results obtained by hardware filtering, a second experiment was performed with a filter of 1 mm aluminium, which is also shown in the line profile graph of figure 11.
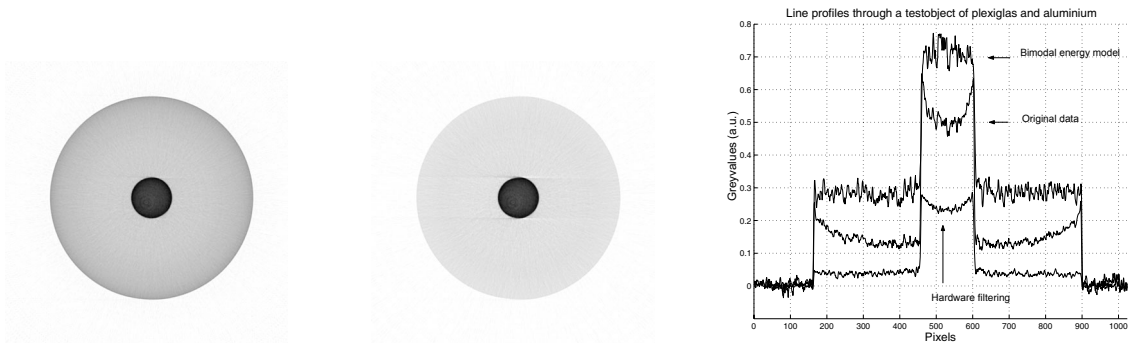

Figure 11. The reconstructed images of a plexiglas cylinder with 10 mm diameter and an aluminium rod of 2 mm in the middle, are shown before (left) and after (middle) beam hardening correction. The scans were done without prefiltering. Note that the greyvalues in the reconstructed images are scaled between zero and their maximum value. The attenuation profiles (right) through these reconstructions are shown and the bimodal energy correction is compared with the results obtained with a 1 mm aluminium hardware filter.

A last test object was created from the femur of a mouse, immersed in a water filled plexiglas cylinder. This test object was scanned with a magnification of 19.83× yielding a pixel resolution of 13.82 μm. The correction method proceeded in the same way as for plexiglas and aluminium. As already mentioned, plexiglas and water have the same attenuation range, thus the beam hardening effect of both materials can be corrected using the curve found for plexiglas. By thresholding the greyvalues in the reconstructed image, the bone was segmented, and the thicknesses were calculated, while the corresponding attenuation values could be found in the sinogram. Figure 12A shows the curve for bone in plexiglas and water at a peak voltage of 80 kVp. We may
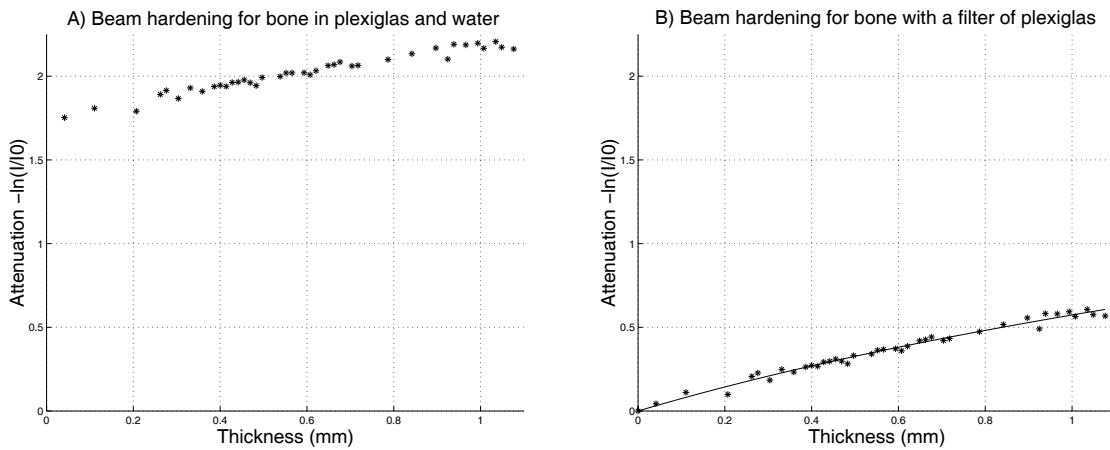
Figure 12. A) The beam hardening curve of bone in plexiglas and water at a peak voltage of 80 kVp. B) We can interpret these data as the attenuation values of bone applying a plexiglas/water filter. This is shown after reducing the values with the attenuation of the thickness of the filter.

consider plexiglas and water as a filter placed between the source and the bone. In figure 12B, the attenuation values of bone were diminished with the attenuation value of the corresponding thickness of plexiglas/water. Now, the beam hardening curves for plexiglas/water and bone are known, the correction is performed. In figure 13, the reconstructed images are shown together with the line profiles through these images, before and after beam hardening correction.
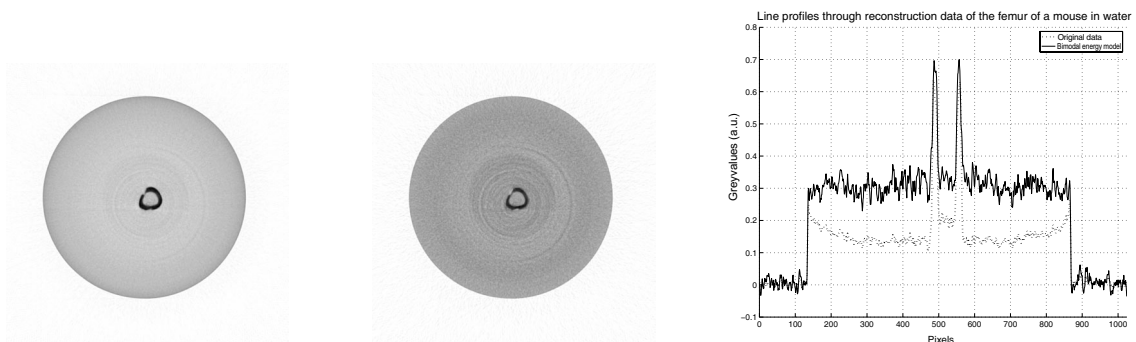

Figure 13. Reconstructed images of a plexiglas holder filled with water and containing the femur of a mouse are shown before (left) and after (middle) beam hardening correction together with the line profiles through these images (middle). Note that the greyvalues in the reconstructed images are scaled between zero and their maximum value.

5. Discussion

The cupping artefact as a consequence of beam hardening can be observed in the reconstruction image of the plexiglas cylinder (figure 5). After correction, the artefacts have disappeared and the image shows a homogeneous object, as it should be. Note that the ringing, due to the differences in pixel sensitivity in the CCD detector, seems to be worse after correction. However, this is a consequence of the contrast enhancement as a result of the projection of every point on the beam hardening curve towards the linear trendline. The ringing artefacts are also present in the original image. In the line profiles through the reconstructed images shown in figure 5, the effect of applying an aluminium filter is also presented. Since plexiglas is a low attenuating material the hardware filter gives a good reduction of the beam hardening artefact. To obtain a quantitative measure of the quality of both correction techniques, the signal to noise ratio (SNR) defined as $20\log\frac{I}{\sigma}$ was calculated, which yield 46.5 dB in the original reconstruction image. This SNR is decreased after correction with the bimodal energy model (41.5 dB) as a consequence of the nonlinear correction procedure. However, the SNR decreases significantly less compared with the use of the aluminium filter (34 dB). By applying a hardware filter, the signal on the detector will decrease, which will result in a lower signal to noise ratio.

The corrected reconstruction image shows the linear attenuation coefficient corresponding with the effective energy E_{eff} of the X-ray source. The slope of the beam hardening curve for thicknesses going to zero will determine the effective energy of the source and the corresponding linear attenuation coefficient μ_{eff}. The tabulated values of the energies and corresponding linear attenuation coefficients can be found at the website of the National Institute of Standards and Technology, NIST‖. For plexiglas,

‖ http://physics.nist.gov/PhysRefData/XrayMassCoef/cover.html

μ_{eff} is calculated as 0.325 mm^{-1} which corresponds with the results shown in figure 5. The corresponding effective energy can be found at the NIST and measures 11.4 kV. In other words, the bimodal energy model gives also a method of measuring the effective energy of the X-ray source spectrum which was a priori not known.

The second two-component system under investigation was the femur of a mouse in air. The reconstruction image was a slice through the top of the bone where, in this case, the bone was hollow (i.e., filled with air). In other words, the same greyvalue outside and inside the bone is expected. In the reconstructed image without beam hardening correction this is clearly not the case (figure 8, dotted line). As a consequence of beam hardening, streak artefacts are obtained, thus since the test object has a closed form, this may be seen as the higher attenuation coefficients of the air inside the bone than the air outside the bone. After beam hardening correction, this effect has disappeared, which is shown in figure 8 (full line). We can conclude that not only the degradation in the intensity inside the bone itself is corrected, also the overestimated value of the air surrounded by the bone is correctly reduced to zero. Note that the remaining streaks in the reconstructed images are not a consequence of beam hardening. Streak artefacts are also caused by misalignment of the source-detector system, or as a consequence of an edge gradient. The misalignment artefacts are corrected using the post-alignment, available on the Skyscan apparatus. The edge gradient streak artefacts, however, frequently occur from the edges between bone and soft tissue. Or, in other words, streak artefacts arise from materials or structures when a high-density material interfaces with a low density material such as air. This can be clearly observed in figure 8. Since the effective energy of the source is known from the previous results for plexiglas, we can find the corresponding linear attenuation coefficient using the tabulated values at the NIST. The μ_{eff} corresponds with 4.43 mm^{-1} which is also found in the correction results

depicted in figure 8.

After the two-component systems discussed above, a combination of plexiglas and water was studied. This is a three-component system (air, water, plexiglas) which can be treated as a two-component system because the attenuation values of both materials are in the same range. Figure 9 shows the results before and after correction with the beam hardening curve for plexiglas. The line profiles show that the cupping artefact is gone after correction and thus the beam hardening effect is clearly reduced. In this case, the contrast between both materials is very low, but nevertheless both materials can be distinguished even better after correction. Note that small differences become larger after projecting the points on the beam hardening curve on to the linear trendline. Thus, in this case, the contrast between water and plexiglas is enhanced which can be seen in the reconstructed image after correction.

An example of two different materials with different attenuation ranges was given in figure 11 for plexiglas and aluminium. Notice that the beam hardening is well compensated for both materials. Thus, the cupping effect has disappeared for plexiglas as well as for aluminium. If we compare these results with the use of an aluminium filter, it is noticed that the beam hardening effect is correctly reduced for plexiglas but not for the aluminium rod. Hardware filtering gives only a reduction of the artefact for high attenuating materials, while our linearization method gives good results for both.

By determining the beam hardening curve of aluminium from a first reconstruction image (figure 10), the environmental artefact is also taken into account [11, 13]. The greyvalues in the image of a certain material do not only depend on the material but also on the environment of the object under examination. In this case, it is not possible to construct the correct beam hardening curve for aluminium using a phantom of Al plates. By determining the beam hardening curves from the obtained greyvalues in the

projection images, the surrounding plexiglas, and thus the environmental problem, is taken into account.

A last correction was done on a four-component system consisting of air, plexiglas, water, and bone. This system can be treated as a three-component system because plexiglas and water attenuate the X-rays in the same energy range. The correction results are shown in figure 13. The bone under investigation was the same sample as discussed before. In other words, the bone was hollow and now filled with water. Because of the beam hardening effect, the attenuation values of water inside the bone are overestimated (streak artefacts). After correction, the attenuation values inside and outside the bone are the same. Furthermore, the beam hardening artefact of plexiglas and water has disappeared, correcting both materials with the curve obtained for plexiglas. Note that the linear attenuation coefficient of the femur of a mouse is lower when scanned in water than scanned in air. This is normal as the X-ray spectrum presented at the bone in air and the bone in water is different. In the latter case, the surrounding plexiglas and water will pre-filter the X-ray spectrum before it reaches the bone. In this way, the effective energy will be increased with respect to the effective energy presented at bone in air. For higher energies, the linear attenuation coefficients will be lower. This can be seen comparing the results of figure 13 with figure 8.

6. Conclusion

The correction method, proposed in this paper, gives good results for different materials and biological test objects. These objects showed three artefacts due to beam hardening: cupping, streaks and environmental artefacts. They are all corrected accurately by the use of the bimodal energy model. Note that some artefacts will remain in the images because they are not caused by beam hardening.

Because of the comparable attenuation of water, plexi and soft tissue, we expect the correction method to work as well for a test object of bone and surrounding soft tissue. The presented correction scheme gives already good results for a composition of different materials. Furthermore, the bimodal energy model was compared to the results obtained by hardware filtering. While hardware filtering gave only a reduction of the artefact, our linearization method presented good results for the different materials. An important advantage of the technique, is the fact that no prior knowledge of the spectrum of the source is required. Furthermore, as a consequence of the physical meaning of the fitting parameters of the bimodal energy model, these may be applied in further research to obtain more information on the used source-detector system.

Acknowledgment

References

[1] R.E. Alvarez and A. Macovski. Energy-selective reconstructions in x-ray computerized tomography. *Physics in Medicine and Biology*, 21(5):733–744, 1976.

[2] R.A. Brooks and G. Di Chiro. Beam hardening in x-ray reconstructive tomography. *Physics in Medicine and Biology*, 21(3):390–398, 1976.

[3] A.J. Duerinckx and A. Macovski. Polychromatic streak artifacts in computer tomography images. *Journal of Computer Assisted Tomography*, 2(4):481–487, September 1978.

[4] M. Van Geet, R. Swennen, and M. Wevers. Quantitative analysis of reservoir rocks by microfocus x-ray computerised tomography. *Sedimentary Geology*, 132:25–36, 2000.

[5] P. Hammersberg and M. Mångård. Correction for beam hardening artefacts in computerised tomography. *Journal of X-ray Science and Technology*, 8(1):75–93, 1998.

[6] G.T. Herman. Correction for beam hardening in computed tomography. *Physics in Medicine and Biology*, 24(1):81–106, 1979.

[7] J. Hsieh, R.C. Molthen, C.A. Dawson, and R.H. Johnson. An iterative approach to the beam hardening correction in cone beam ct. *Am. Assoc. Phys. Med.*, 27(1):23–29, 2000.

[8] R.J. Jennings. A method for comparing beam hardening filter materials for diagnostic radiology. *Medical Physics*, 15:588–599, 1988.

[9] P.M. Joseph and C. Ruth. A method for simultaneous correction of spectrum hardening artifacts in ct images containing both bone and iodine. *Medical Physics*, 24(10):1629–1634, October 1997.

[10] P.M. Joseph and R.D. Spital. A method for correcting bone induced artifacts in computed tomography scanners. *Journal of Computer Assisted Tomography*, 2(1):100–108, January 1978.

[11] P.S. Rao and R.J. Alfidi. The environmental density artifact: a beam-hardening effect in computed tomography. *Radiology*, 141:223–227, October 1981.

[12] E. Van de Casteele, D. Van Dyck, J. Sijbers, and E. Raman. An energy-based beam hardening model in tomography. *Physics in Medicine and Biology*, 47(23):4181–4190, December 2002.

[13] S.W. Young, H.H. Muller, and W.H. Marshall. Computed tomography: Beam hardening and environmental density artifact. *Radiology*, 148:279–283, July 1983.

[14] L.M. Zatz and R.E. Alvarez. An inaccuracy in computed tomography: The energy dependence of ct values. *Radiology*, 124:91–97, July 1977.